ACS OMEGA

http://pubs.acs.org/journal/acsodf

Article

Anchoring of Nanocomposites Based on Novel Metal Nanocomplexes/Nanocarbonaceous Surfaces and Assessing Their In Vivo Anticancer Effects on Ehrlich Ascites Tumor

Heba Bassiony Ghanem,* Rehab Galal El-Sharkawy, and Rania Hosny Taha

Cite This: *ACS Omega* 2022, 7, 41627−41640

Read Online

ACCESS | Metrics & More | Article Recommendations

ABSTRACT: Nanotechnology is the study of materials' unique properties at the nanoscale. Nanomedicine is the application of nanotechnology in medicine, which has been utilized to treat some common diseases, such as cancer. The **aim** of the present work is to synthesize the cadmium (Cd) nanocomplex using paracetamol as a ligand with a molar ratio of 1:2 M/L that was characterized by different physicochemical methods and to explore the effect of the synthesized Cd nanocomplex on the immune system and the redox status of the body and their anticancer effects on Ehrlich ascites carcinoma (EAC) induced in mice. Eighty female albino mice were separated into **Group I:** control; **Group II:** EAC; **Group III:** EAC treated with a low-dose Cd nanocomplex; and **Group IV:** EAC treated with a high-dose Cd nanocomplex. Interleukin-6 (IL-6), NLR family pyrin domain containing 3 (NLRP3), and 8-hydroxy 2-deoxyguanosine (8-OHdG) levels were assessed by enzyme-linked immunosorbent assay (ELISA). Peroxynitrite level and glutathione peroxidase activity were assessed by spectrophotometry. NRF2 mRNA expression, cadmium content, and liver and renal toxicity were estimated. **Results:** There was a significant increase in IL-6, NLRP3, 8-OHdG, peroxynitrite, and NRF2 mRNA expressions and in the glutathione peroxidase activity in EAC treated with low- and high-dose Cd nanocomplexes. However, the EAC treated with high-dose Cd nanocomplex group showed significant liver and renal toxicity. **Conclusion:** Cadmium nanocomplex has anticancer effects on EAC induced in mice via **its effects** on the immune system and redox status as well as pyroptosis and epigenetic instability of the body, while high doses of Cd nanocomplex can cause liver and renal toxicity.

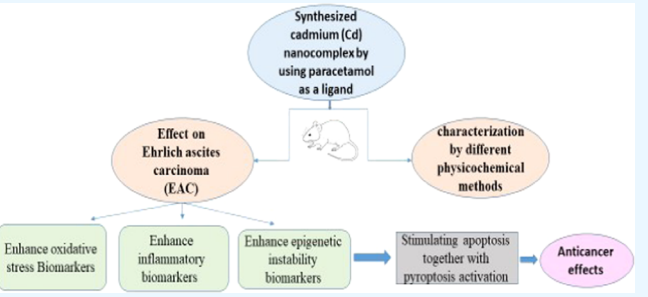

1. INTRODUCTION

Acetaminophen (*N*-acetyl-*p*-aminophenol, paracetamol (Para)) (Figure 1) is a medication that has good analgesic and antipyretic properties.[1,2] Taking the presumed molecular mechanisms of hepatotoxicity and the analgesic activity of paracetamol into consideration, there have been several attempts to enhance its analgesic activity while preventing its toxicity by modifying its structure.[3,4] There was an attempt to enhance the analgesic activity of the drug by monosubstitution ortho to the hydroxyl group.[4] According to a literature review, studies on metal complex production employing pharmaceuticals as ligands have received a lot of interest in the last decade.[5] Metal ions have the ability to easily lose electrons from their known elemental or metallic state, resulting in positively charged ions. In the discovery of novel pharmaceutical molecules, metal-containing compounds have numerous benefits over traditional carbon-based chemicals. The biological applications of these metal complexes, such as

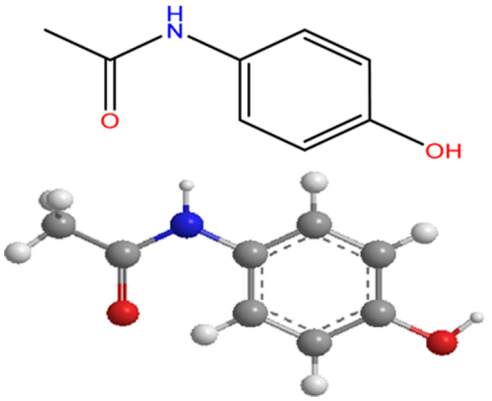

Figure 1. Paracetamol (Para) drug structure.

Received: August 31, 2022
Accepted: October 26, 2022
Published: November 4, 2022

https://doi.org/10.1021/acsomega.2c05631
ACS Omega 2022, 7, 41627−41640

antifungal, antibacterial, and antitumor properties, have made them particularly fascinating.[6] These complexes offer great diversity in their action; they not only have anticancer properties but have also been used as antibacterial, anti-inflammatory, and antidiabetic compounds.[7]

Montmorillonite (MMT) is one of the most closely utilized layered silicates for the creation of nanocomposites.[8] A principal framework of two silicon tetrahedral SiO_4^{4-} sheets and one aluminum octahedral ($Al(OH)_6^{3-}$) sheet is essential for the unit crystal structure of Mt.[9] Owing to the Mg^{2+} substitution for Al^{3+}, the Mt surfaces have negative charges. These negative charges are counter-balanced by the first cation group (e.g., sodium) in proximity to the clay layers inside the sp-interlayer spaces.[10] The polarity in the pristine system (Na^+MMt) is caused by these charges, making the silicate layers with a large number of organic polymers.[11] To develop or lower the hydrophilicity of the layered silicates, numerous mechanisms were checked. The ion-exchange reactions between alkylammonium salts and Na^+ ions in MMT layers by means of cation-exchange procedures are recognized as some of the many technically attractive and enhancing techniques.[8] The modulation of the MMT surfaces with chitosan is capable of improving the chemical reaction with the organic resin. Modulation via chemical methods is overwhelmingly utilized to make chemical bonds at the surface. Chitosan grafting of Na^+MMT takes place on the inner and outer surfaces of sheets.[12]

Furthermore, nanotechnology is the study of materials' unique properties at the nanoscale (1−100 nm). Nanomaterials contain unique optical, electrical, and/or magnetic properties that can be employed in a variety of applications, including electronics and medicine. The word "nanomedicine" is used to describe the use of nanotechnologies in medicine and healthcare. Nanomedicine, in particular, employs nanoscale technologies and nanoenabled approaches to prevent, diagnose, follow up, and manage diseases such as cardiovascular disease, autoimmune diseases, and cancer.[13,14]

Cancer is currently one of the most widely predominant topics in science and technology research. Cancer is the world's second biggest cause of death, with over 9 million fatalities in 2018. Cancer is caused by abnormalities in the cell, which cause it to develop abnormally and create a tumor. Cancer cells spread to other parts of the body via blood and lymphatic channels, generating a tumorigenic mass of cells. For decades, experts have been focused on early cancer detection and successful therapy. Ehrlich carcinoma is one of the most prevalent experimental cancers, and it is extremely important for modeling purposes. Ehrlich ascites carcinoma (EAC) is a spontaneous murine mammary cancer that is hyperdiploid at the outset and can transplant intraperitoneally passages on all mouse strains.[15]

Chemotherapy is the most frequent cancer treatment method that involves inducing apoptosis in cancer cells. It has a significant impact on patients' lives and is believed to be a leading cause of mortality.[16] Chemotherapy for cancer management is generally linked with side effects such as the death of healthy cells and low bioavailability of synthetic chemotherapeutic medications; hence, research into more efficacious chemotherapeutic agents that are less damaging to normal cells is critical.[17]

Nanoparticles have recently been used in anticancer therapy in an effort to better target delivery systems and limit damage to healthy cells. Metal nanoparticles have sparked a lot of interest in recent years due to their unique physical, chemical, and biological features, and they have quickly become the most productive research area.[18]

Cadmium nanocomplexes have unique chemical, optical, photoelectrochemical, and electrical features, including fluorescence, high-resolution second harmonic production, and two photon-emissions, making them effective anticancer agents.[19] Cadmium nanocomplexes have also been established to cause apoptosis in cancer cells by preventing the repair of DNA and generating free-radical-induced DNA damage, mitochondrial damage, and disruption of intracellular calcium signaling, making them essential for cancer cell targeting. Cadmium nanocomplexes kill cancer cells primarily by protein, DNA, and cell-wall destruction.[20] Additionally, a recently discovered programmed cell death pathway with intrinsic inflammatory effects known as pyroptosis is caspase-1-mediated cell death that can mainly be regulated by cadmium nanocomplexes. Pyroptosis is different from other forms of cell death in morphology and mechanism and has a vital role in cancer management.[21]

The present project aims to synthesize cadmium (Cd) nanocomplexes using paracetamol as a ligand with a molar ratio of 1:2 M/L, which was characterized by different physicochemical methods and also to explore the effect of the synthesized Cd nanocomplex on the immune system and redox status of the body and its anticancer effects on Ehrlich ascites carcinoma (EAC) induced in mice.

2. EXPERIMENTAL SECTION

2.1. Materials. Acetaminophen (*N*-acetyl-*p*-aminophenol (Para), paracetamol), $CdCl_2{\cdot}H_2O$, dimethylformamide (DMF), etc. were purchased from Aldrich and used without purification.

The coupling agent, chitosan (Ch), was obtained from Across Organics and was used as received. Montmorillonite (Southern Clay Products) with 6.39% Fe3C, 0.88% Mg2C, 15.50% Al3C, and 77.28% Si4C was used. Montmorillonite/Na (Na\MMt) was prepared by immersing the clay into a sodium chloride solution of 1.0 M. The sample was immersed in double-distilled water and centrifuged at 60 000 rpm. The process was carried out many times, and the Cl-free samples were left to dry at room temperature. According to the BaCl2 process, the cation-exchange capacity (CEC) of clay in NaC is 110 meq\100 g.[22]

2.2. Methods. The ^1H and ^{13}C NMR spectra in DMSO-d_6 were recorded on a 600MHZ spectrometer without using an internal standard. Thermal analyses were carried out using the thermogravimetric analyzer in a dynamic nitrogen atmosphere at the heating rate of 10 °C/min in the central laboratory at Jouf University. The conductivity was measured on a JEN WAY 4510 conductivity meter using DMF as the solvent at room temperature. Elemental analysis (C, H, N, S) was performed using an EL-elemental analyzer.

2.3. Synthesis of Cd Nanocomplexes. To prepare Cd nanocomplexes, a solution of an appropriate amount of ligand (0.005 mmol) in 10 mL of chloroform/methanol 2:1 (V/V) was added to a solution of metal (II) chloride (0.0025 mmol) in 10 mL of methanol.

The solution was placed in a Teflon-lined stainless steel autoclave, which was heated to 450 °C for 24 h before being cooled to ambient temperature. The final product was filtered, dried, and characterized. The isolated complex was powdered, was stable in air, soluble in DMF and dimethyl sulfoxide

https://doi.org/10.1021/acsomega.2c05631
ACS Omega 2022, 7, 41627−41640

(DMSO), and insoluble in most organic solvents, and its elemental analysis is in accordance with the proposed stoichiometry and agrees well with the suggested molecular formula.

2.4. Synthesis of Nanomaterials. A total of 3 g of Na-MMt was distributed into 150 mL of water for 24 h, followed by the addition of 50 mL of chitosan (Cs) (0.5% in 1% acetic acid), and then, the mixture was stirred for 6 h. The Na-MMT modified by Cs (Na-MMT/Cs) was filtered and washed with a mixture of water/ethanol and then dried at 60 °C in a vacuum oven for 12 h.

For the synthesis of Na-MMT/Cs/Cd, 2 g of Na-MMT/Cs was added to 50 mL of Cd-complex dissolved in DMF at 80 °C under reflux with vigorous stirring for 3 h. The dark powder was filtered and washed several times with distilled water and methanol until the filtrate turned colorless. The dark powder was dried in an oven at 60 °C for 24 h. The same procedure was applied for the synthesis of sodium montmoronlite/graphene oxide/chitosan/Cd (Na-MMT/go/Cs/Cd).

2.5. Cd Nanocomplex Effect on Ehrlich Ascites Carcinoma (EAC) Experiment. *2.5.1. Experimental Animals.* The study used 80 female albino mice that were 9−12 weeks old and weighed 30−45 g. All of the animals were housed in wire mesh cages and given frequent chews as well as free access to water. During the study, they were kept in standard conditions of temperature (252 °C) and a 12 h light/dark cycle. The study was performed in the Medical Biochemistry department, Faculty of Medicine, Tanta University. The study followed the National Institutes of Health's Health Guide for the Care and Usage of Laboratory Animals (NIH publication number 8523, revised in 1996). The study was approved by the Research Ethics Committee of the Faculty of Medicine, Tanta University, with the approval code 35894/10/22.

2.5.2. Experimental Design and Animal Grouping. 2.5.2.1. Experimental Design. In this work, an Ehrlich ascites carcinoma (EAC) cell line was employed. The initial line was obtained from Cairo University's National Cancer Institute. An intraperitoneal (i.p.) puncture with a sterile insulin syringe was used to extract Ehrlich carcinoma cells. The extract was subsequently diluted in 0.9 percent sterile saline (1:9 v/v). The number and viability of EAC cells per ml of this suspension were counted using a hemocytometer and trypan blue dye under a microscope.[23] To generate a liquid tumor, the EAC cells (1×10^6) in the ascites fluid were collected from a stock mouse and injected into the mice (i.p.) in 0.1 mL of phosphate-buffered saline (PBS).[23]

2.5.2.2. Experimental Groups. The mice were separated into four groups of 20 mice each after they had been adapted for one week.

Group I was the **Control group**, in which the mice were injected i.p. by 0.1 mL of phosphate-buffered saline (PBS) once and observed for 36 days.[24]

Group II was the **Ehrlich ascites carcinoma (EAC) group**, in which the mice were given 1×10^6 EAC cells once through i.p. injection in 0.1 mL of PBS and observed for 36 days.[24]

Group III was the **EAC treated with low-dose cadmium (Cd) nanocomplex group**, in which the mice received the **Cd nanocomplex** orally (0.5 mg kg^{-1}) once daily for 36 days after implantation of EAC.[25]

Group IV was the **EAC treated with high-dose cadmium (Cd) nanocomplex group**, in which the mice received the **Cd nanocomplex** orally (2 mg kg^{-1}) once daily for 36 days after implantation of EAC.[25]

2.5.3. Tissue Sampling and Homogenate Preparation. At the end of the present study (36 days), mice were given general anesthesia and ascites fluid was collected using sterile syringes; the anticarcinogenic impact of the Cd nanocomplex was also evaluated by performing a cell count for ascetic fluid using a hemocytometer and trypan blue dye to evaluate tumor growth.[23] By comparing the cell count of cancer cells and ascites fluid volume in the peritoneal cavity of treated and control groups, the growth inhibition of cancer cells was estimated. The ascites fluids were then centrifuged at 4 °C for 20 min at a speed of 4000 rpm to collect tumor cells, which were then stored at −80 °C for further investigations. The residual ascites fluids were stored at −80 °C. All of the mice were sacrificed, and blood samples were collected in plain tubes and centrifuged for 15 min at 4000 rpm at 4 °C to obtain serum samples. Liver and renal tissues were excised and wrapped in aluminum foil before being preserved at −80 °C until they were utilized to test the therapy's toxicity. With a Potter−Elvenhjem tissue homogenizer, the EAC cell lysate was made using 10 mM potassium phosphate buffer pH 7.4 in the ratio of 1/5 (w/v). The crude lysate was centrifuged for 15 min at 4 °C at 4000 rpm.

2.5.4. Biochemical Assays. 2.5.4.1. Measurement of Cadmium Content in EAC. Inductively coupled plasma mass spectrometry (ICP-MS) was used to determine the cadmium levels in EAC cells, liver, and renal tissue samples (model: Optima 7000 DV, Perkin Elmer, Germany). The assessment was carried out according to Takahashi et al.'s technique (mentioned in the 2000s).[26]

2.5.4.2. Enzyme-Linked Immunosorbent Assay (ELISA) Parameters.

a. **Mouse Interleukin-6 (IL-6) level** as the inflammatory marker in the EAC lysate was assayed quantitatively following the manufacturer's instructions of the ELISA kit (Sigma RAB0308) provided by Sigma-Aldrich Company.
b. **Mouse NLR family pyrin domain containing 3 (NLRP3) level** as the pyroptosis marker in the EAC lysate was measured using a commercial ELISA kit supplied by Abcam Company, Cat. number ab279417.
c. **Mouse 8-Hydroxy 2-Deoxyguanosine (8-OHdG) level** for epigenetic instability in the EAC lysate was evaluated to assess epigenetic instability using the ELISA technique performed according to commercial kits supplied by MyBioSource, Inc. Company (Cat No. MBS263767).

2.5.4.3. Spectrophotometric Assay.

a. **The Bradford method was used to determine the protein concentration** in plasma and EAC cell lysate. The quantities of total proteins in the samples were determined using the Bradford method (BioRad protein assay #Cat 5000006).[27]
b. **Oxidative stress in EAC lysate** was determined by evaluation of the **peroxynitrite level** according to the method described by Beckman et al. (1992)[28] and cited by VanUffelen et al. (1998).[29] The nitration of phenol by peroxynitrite results in nitrophenol, which can be detected spectrophotometrically at 412 nm. The results were expressed in μmol/g tissue.

https://doi.org/10.1021/acsomega.2c05631
ACS Omega 2022, 7, 41627−41640

Table 1. Primer Sequences of NRF2 Gene Expression

gene	forward	reverse
Nrf2	5′ TTGGCAGAGACATTCCCATTTG 3′	5′ AAACTTGCTCCATGTCCTGCTCTA 3′
β-actin	5′ GTCCCTCACCCTCCCAAAAG 3′	5′ GCTGCCTCAACACCTCAACCC 3′

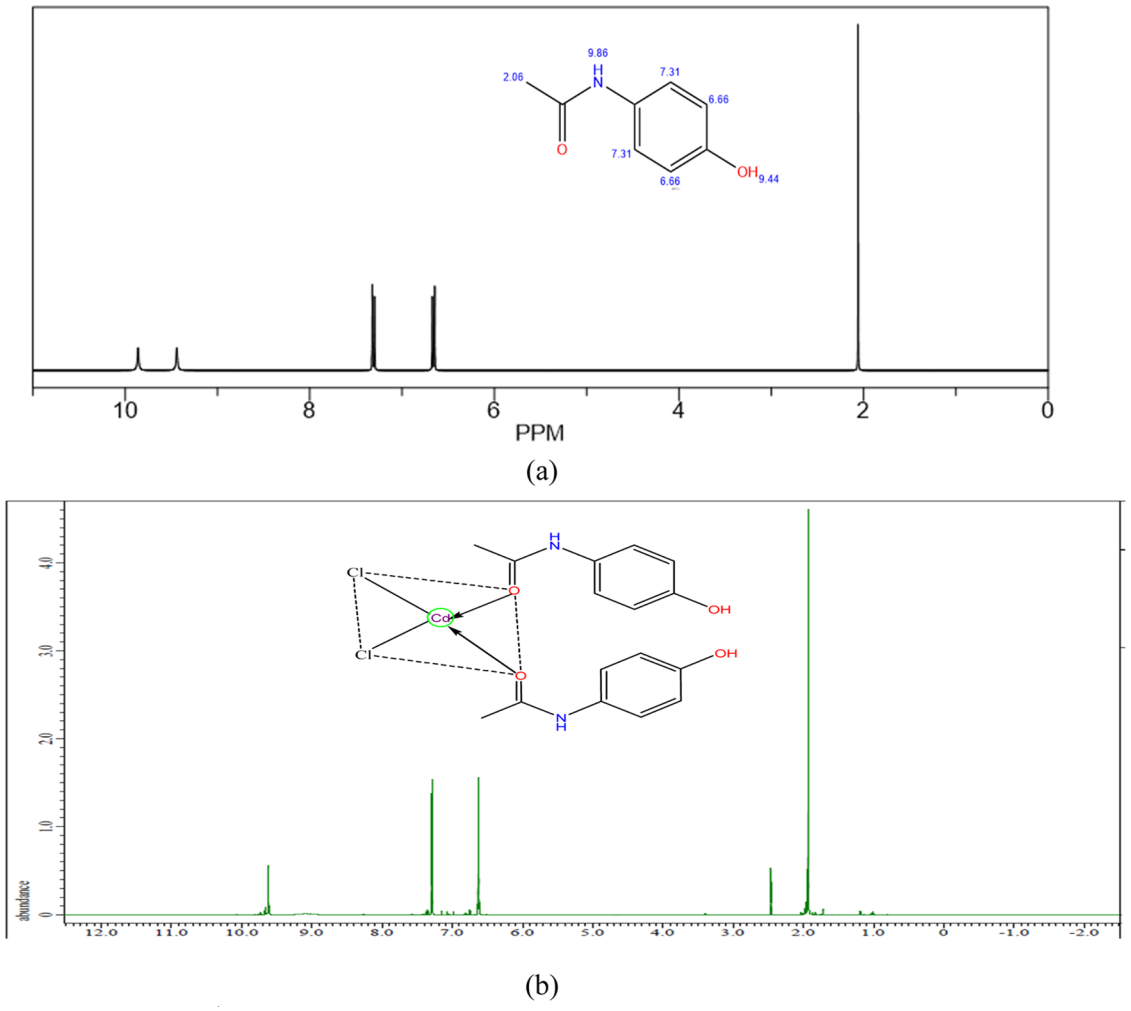

Figure 2. ^{1}H NMR spectra of (a) the free ligand and (b) the Cd-complex.

c. **Antioxidant activity of glutathione peroxidase in EAC lysate** was assessed using a colorimetric kit provided by BIODIAGNOSTIC Company, Egypt, as per the method described by Paglia DE (1967).[30]
d. **Renal toxicity in plasma** was assessed using a commercial kit from Egypt's BIODIAGNOSTIC Company to evaluate creatinine and blood urea nitrogen (BUN) levels.
e. **Liver toxicity in plasma** was estimated by measuring the activities of aspartate transaminase (AST) and alanine transaminase (ALT) using the commercial kit from BIODIAGNOSTIC Company, Egypt.

2.5.4.4. Quantitative Measurement of NRF2 mRNA Expression by Quantitative Real-Time Reverse Transcription Polymerase Chain Reaction (RT-PCR). The manufacturer's protocol was followed to separate the total RNA from EAC using the Gene JET RNA Purification kit (# K0731, Thermo Scientific). The total RNA (5 g) was reverse-transcribed to create cDNA using Revert Aid H Minus Reverse Transcriptase (#EP0451, Thermo Scientific), as previously demonstrated by El-Magd et al. (2017).[31]

The cDNA was utilized as a template to determine the relative expression of the NRF2 gene using Step One Plus real-time PCR equipment (Applied Biosystems). Primer 5.0 software was used to construct the primers, and their sequences are as shown in Table 1.

A total of 2 μL of cDNA template, 12.5 μL of 2X Maxima SYBR Green/ROX qPCR Master Mix (# K0221, Thermo Scientific), 1 μL of forward primer, 1 μL of reverse primer, and 8.5 μL of nuclease free water were used and mixed together to make a 25 μL PCR mix. Initial denaturation at 95 °C for 10 min, 40−45 cycles of DNA amplification at 95 °C for 15 s, annealing at 60 °C for 30 s, and extension at 72 °C for 30 s were used. The temperature was raised from 63 to 95 °C for melting curve analysis by the end of the final cycle. For target genes and the housekeeping gene, the cycle threshold (Ct) values were determined, and the relative gene expression was determined using the $2^{-\Delta\Delta Ct}$ method.[32]

https://doi.org/10.1021/acsomega.2c05631
ACS Omega 2022, 7, 41627−41640

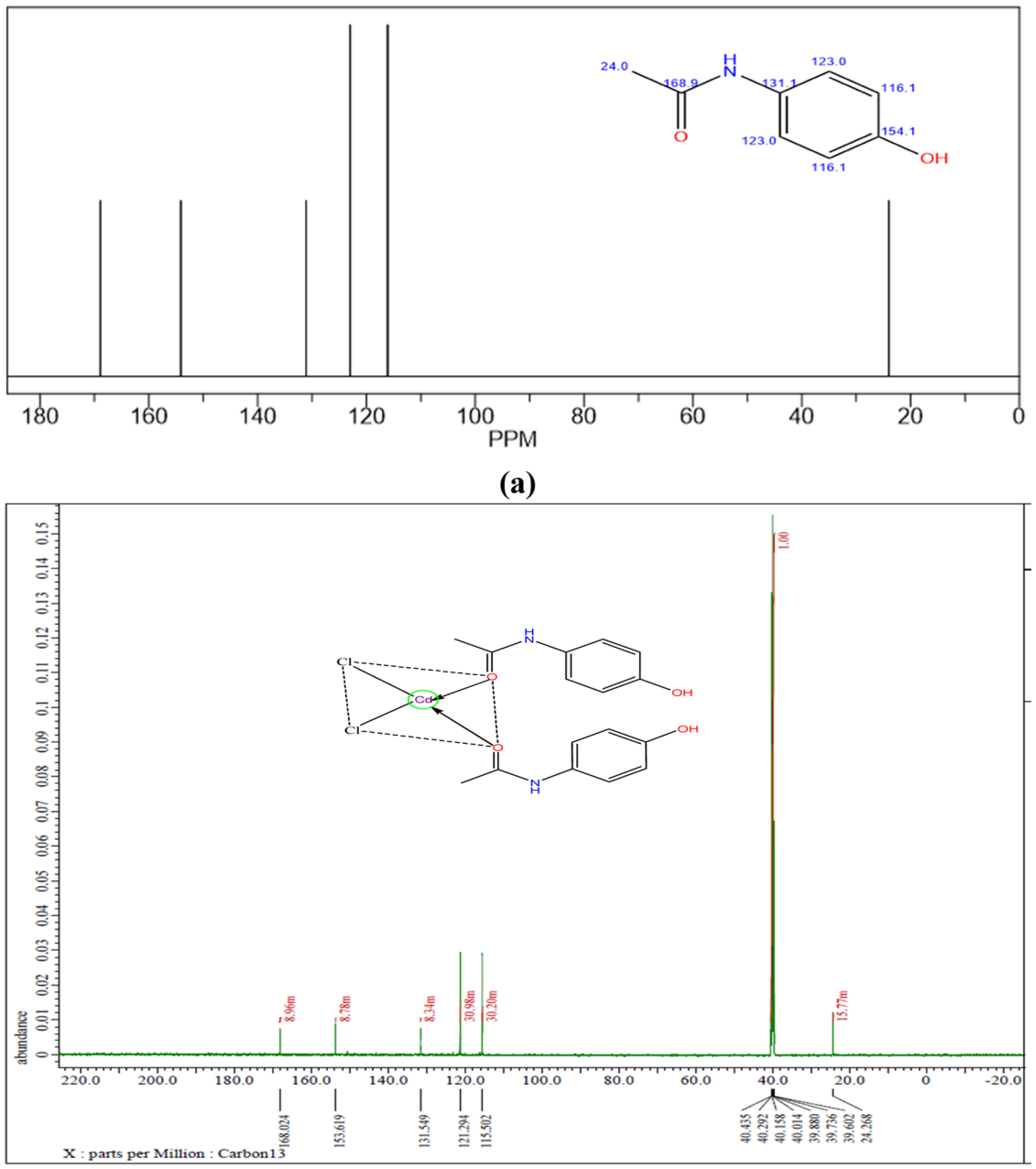

Figure 3. ^{13}C NMR spectra of (a) the free ligand and (b) the Cd-complex.

2.5.5. Statistical Analysis. The entire set of data was presented as means ± standard deviation (SD). The statistical significance was calculated using one-way analysis of variance (ANOVA) and SPSS 23.0 software. When $P \leq 0.05$, *P*-values were considered statistically significant. Tukey's HSD (Tukey's honestly significant difference) test was used to compare the means. The ΔCt values of the test genes were standardized to the ΔCt of the calibrator

$$\Delta\Delta Ct = \Delta Ct\ (test) - \Delta Ct\ (calibrator)$$

The relative gene expression fold change was calculated as follows

$$\text{Fold change} = (2^{-\Delta\Delta Ct})$$

3. RESULTS AND DISCUSSION

The prepared Cd-complex afforded the mononuclear metal complex. The data from elemental analysis suggest that the synthesized metal complex has a 1:2 (M/L) stoichiometry with the molecular formula $[M(Para)_2(Cl)_2]$. The molar conductance falls in the expected range of nonelectrolyte nature.

The ^1H NMR spectrum of the free drug shows a singlet peak at 9.44 ppm, in addition to another singlet signal at 9.86 ppm and multiplet signals at 6.66−7.31 ppm. However, the ^1H NMR data of the metal complexes display singlet peaks at 9.58 and 9.50 ppm for Ag and Cd complexes, respectively. Moreover, the spectra of the complexes showed multiplet signals at 6.63−7.27 ppm.

The ^1H NMR spectrum of the free drug shows a singlet peak at 9.44 ppm, which can be assigned to the OH proton, in addition to another singlet signal at 9.86 ppm due to the NH proton and multiplet signals at 6.66−7.31 ppm due to the

https://doi.org/10.1021/acsomega.2c05631
ACS Omega 2022, 7, 41627−41640

Table 2. ^{13}C Chemical Shifts (in ppm) for the Free Ligand and the Cd Complex

carbon	^{13}C chemical shift for the free ligand	^{13}C chemical shift for the Ag nanocomplex	assigned to
1	154	153.5	C of the benzene ring
2	158.9	168.2	C of the carbonyl group
3	24.0	24.31	C of the methyl group
4	116	115.48	C of the benzene ring
5	123	121.87	C of the benzene ring
6	131.1	131.49	C of a benzene ring attached to the NH group

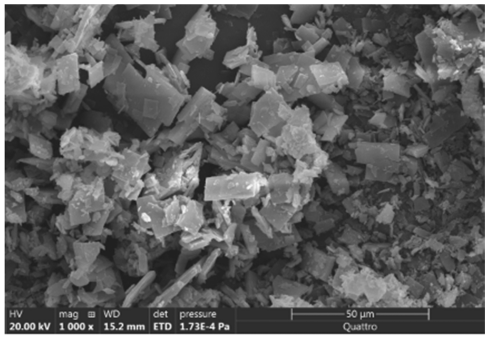

Figure 4. SEM image of the Cd-complex.

aromatic protons. By a careful comparison of the ^{1}H NMR data of the metal complex with that of the free ligand, it was found that the spectrum of the metal complex displays a shift of the singlet peak attributed to the NH group to 9.50 ppm, indicating the involvement of the ketonic group in coordination with the metal atom. Moreover, the spectrum of the complex showed multiplet signals at 6.63−7.27 ppm, which can be due to the aromatic protons, while there is no change in the OH protons (Figure 2a,b).[33]

The ^{13}C NMR spectra of the free ligand and the metal complexes were recorded in DMSO-d_6 (Figure 3). The measured chemical shifts of all C atoms are listed in Table 2. By careful comparison, it was indicated from the data that there is no shift in all carbon atoms except for that of the carbonyl group, indicating the participation of the oxygen of the carbonyl group only in complexation.[13]

At room temperature, the molar conductivities of the 10^{-3} M solution of the metal complex (Λm) were discussed and measured. The data obtained reveal that the metal complex is nonionic (neutral) in nature, which confirms the coordination mode of chlorides with the metal cations, suggesting the nonelectrolyte nature of the complex.

The microstructure of the Cd-complex has been investigated using the scanning electron microscope (SEM) technique, with the corresponding image presented in Figure 4.

The particle size was found to be around 65 nm, with the particles being both cubic and spherical. Although different methods have been applied to prepare nanoparticles, this report is a scarce report on the synthesis of the Cd-complex.[34]

Correlation of all results obtained for the metal complexes under study gives us information regarding the suggested structures of the complexes, as shown in Figure 5.

Fourier transform infrared (FTIR) spectroscopy was used to depict the existence of particular chemical groups in the structure of ingredients and the interlinkage among macromolecular chains and modulated clay.[35] The synthesized nanocomposites MMT\(Ch), MMT\go\(Ch), and MMT\go\(Ch) CdNPs were featured utilizing FTIR. The FTIR results show the interaction among chitosan, clay, and Cd-nanoparticles within the synthesized nanocomposites. The distinctive advantage of clay is that it includes molecules like SiO_2, Al_2O_3, and Mg−O. When checking the FTIR spectra of MMT\(Ch), it was noted that the O−H stretch vibration appeared at 3619 cm^{-1}, which shows the growing hydrogen bonding between the lattice hydroxyls and organic groups.[36] Also, the N−H peak and the O−H stretching height from chitosan and the O−H stretch plateau from clay merged and transformed into this broad peak at ∼3620 cm^{-1}. Also, the peak at 1030 cm^{-1} (symmetric C−O at C−O−C bonds) in chitosan interferes with the peak at ∼1008 cm^{-1} (Si−O stretch) of clay. The O−H bending vibration appeared at 1510 cm^{-1}, the Si−O stretching was located at 997 cm^{-1}, the bending vibration was at 513 cm^{-1}, the Al−OH vibration was at 916 cm^{-1}, and the Mg−O vibration was at 796 cm^{-1}. Clay peaks were noted in the spectra of MMT\(Ch), as mentioned previously.[37] However, protons within the chitosan are hydrogen-bonded oxygen species of SiO and AlO segments; SiO and AlO bonds might be diminished, and the tetrahedral symmetry of these fragments may be deformed. The small peak at ∼789 cm^{-1} coincides with the vibration of the saccharide structure of CS.

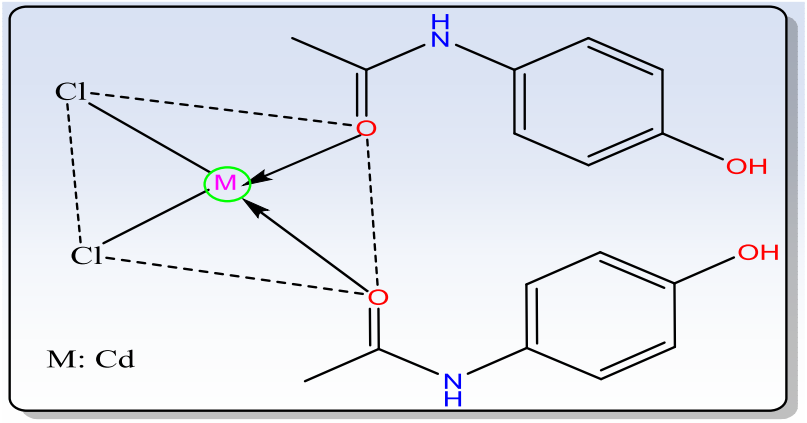

Figure 5. Paracetamol metal complex.

https://doi.org/10.1021/acsomega.2c05631
ACS Omega 2022, 7, 41627−41640

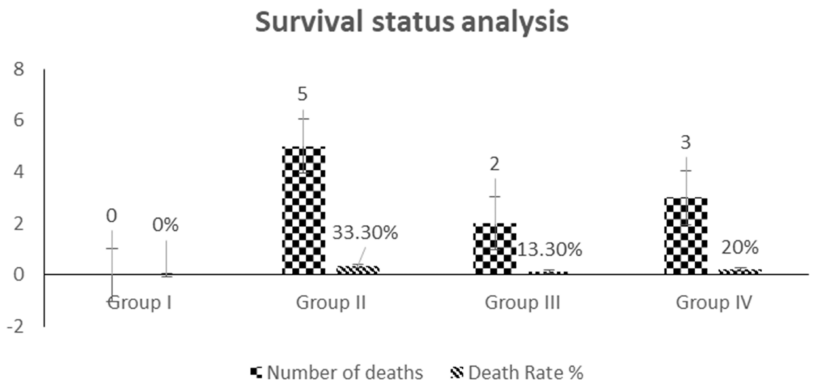

Figure 6. Survival status analysis (after 36 days). Group I: Control group; Group II: Ehrlich ascites carcinoma (EAC) group; Group III: EAC treated with low-dose Cd nanocomplex group; and Group IV: EAC treated with high-dose Cd nanocomplex group.

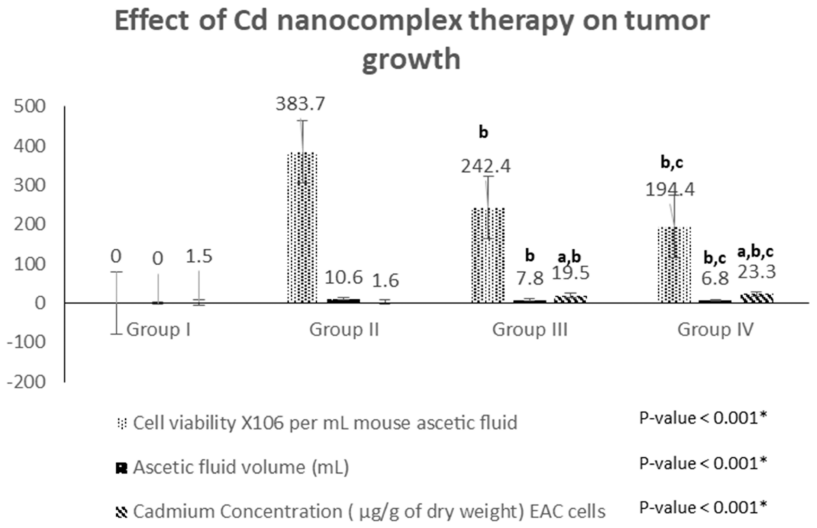

Figure 7. Effect of Cd nanocomplex therapy on tumor growth in the studied groups. Values are expressed as mean ± SD. Number of rats in each group (n = 15). P was considered significant at <0.05. (a) Significance vs group I, (b) significance vs group II, and (c) significance vs group III using one-way ANOVA followed by Tukey's post hoc test for multiple comparison.

Table 3. Correlation between Cadmium Concentrations in EAC Cells and EAC Viability & Ascites Fluid Volume among Different Studied Groups[a]

	cadmium concentrations		EAC viability		ascites fluid volume	
	r.	*P*	*r.*	*P*	*r.*	*P*
cadmium concentrations in EAC cells			−0.58	0.001*	−0.39	0.034*
EAC viability	−0.58	0.001*			0.52	0.003*
ascites fluid volume	−0.39	0.034*	0.52	0.003*		

[a]P was considered significant at <0.05.

Also, the interaction between MMT\chitosan and Go was studied. The synergistic effect on the chitosan properties upon adding both MMT nanoparticles and graphene oxide was observed by FTIR. Both peaks at 1602 cm^{-1} are related to the $-NH_2$ absorbance vibration, and at 1718 cm^{-1}, they belong to the C═O stretch of the carboxylic group.

The C−O stretching at 1028 cm^{-1} of pure chitosan is approximately disappearing. The FTIR results after the addition of Cd are represented in Figure 3. It is noticed that the Cd loaded showed either a shift or a reduction in peaks, suggesting the vital role played by the functional groups. There are some shifts in the absorbance peaks after the addition of Cd such as the peak at 3620 cm^{-1} becoming less broad and the $-NH_2$ peak shifting to ∼1635 cm^{-1}; the C−O stretching of pure chitosan clearly appears at ∼1028 cm^{-1}. These shifts in the wavelength showed that there was a metal-binding process taking place at the surface. The appearance of the peaks located at ∼516 cm^{-1} and the shift of the peaks at 609 cm^{-1} after the addition of Cd were due to the loading effect of the metal.

In the same context, Ehrlich solid tumor is a mimicked breast cancer and a spontaneous mammary adenocarcinoma in mice.[38] The Ehrlich solid tumor has been utilized as a transplantable tumor model to study the anticancer effects of a variety of chemical substances.[39] Ehrlich ascites carcinoma (EAC) is a mammary adenocarcinoma that develops spontaneously in mice and is characterized by fast proliferation, undifferentiation, a reduced life span, and 100% malignancy. EAC resembles human cancers because of these characteristics.[40]

Nanotechnologies, which are largely based on nanoparticles, can help with cancer treatment delivery. Controlling drug cytotoxicity using nanoparticle-mediated drug delivery relies

https://doi.org/10.1021/acsomega.2c05631
ACS Omega 2022, 7, 41627−41640

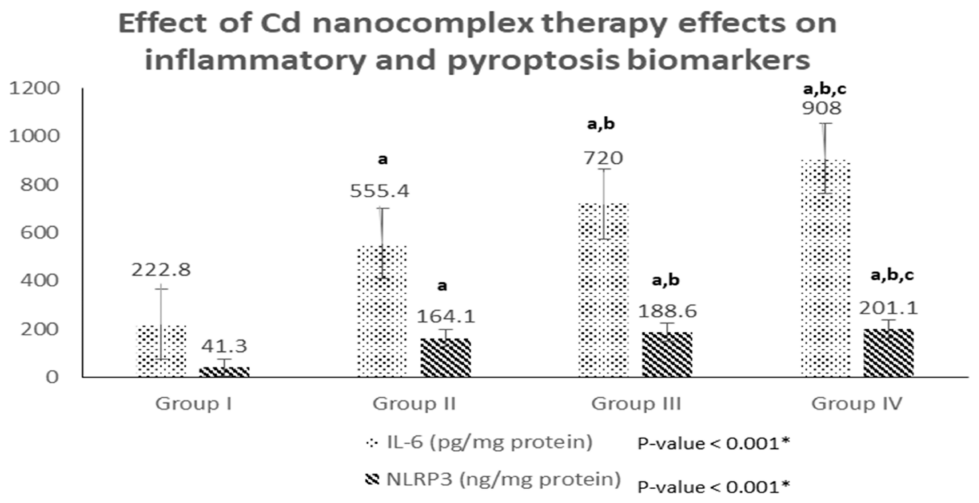

Figure 8. Effect of Cd nanocomplex therapy on inflammatory and pyroptosis biomarkers in the studied groups. Values are expressed as mean ± SD. Number of rats in each group (n = 15). P was considered significant at <0.05. (a) Significance vs group I, (b) significance vs group II, and (c) significance vs group III using one-way ANOVA followed by Tukey's post hoc test for multiple comparison.

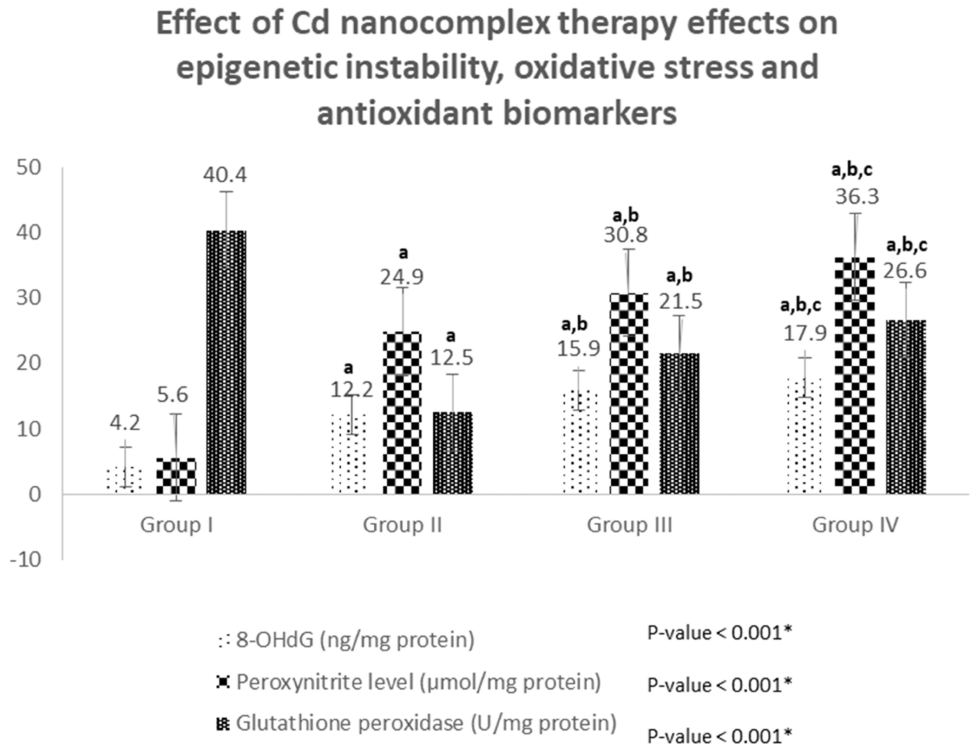

Figure 9. Effect of Cd nanocomplex therapy on epigenetic instability, oxidative stress, and antioxidant biomarkers in the studied groups. Values are expressed as mean ± SD. Number of rats in each group (n = 15). P was considered significant at <0.05. (a) Significance vs group I, (b) significance vs group II, and (c) significance vs group III using one-way ANOVA followed by Tukey's post hoc test for multiple comparison.

Table 4. Correlation between Different Studied Biomarkers among the Different Studied Groups

	IL-6(ng/mg protein)		HMGB1 (pg/mg protein)		8-OHdG (pg/mg protein)		peroxynitrite level (mmol/mg protein)		glutathione peroxidase	
	r.	*P*	*r.*	*P*	*r.*	*P*	*r.*	*P*	*r.*	*P*
IL-6(ng/mg protein)			0.836	<0.001*	0.840	<0.001*	0.883	<0.001*	0.903	<0.001*
HMGB1 (pg/mg protein)	0.836	<0.001*			0.719	<0.001*	0.750	<0.001*	0.863	<0.001*
8-OHdG(pg/mg protein)	0.840	<0.001*	0.719	<0.001*			0.766	<0.001*	0.813	<0.001*
peroxynitrite level (mmol/mg protein)	0.883	<0.001*	0.750	<0.001*	0.766	<0.001*			0.844	<0.001*
glutathione peroxidase (U/mg protein)	0.903	<0.001*	0.863	<0.001*	0.813	<0.001*	0.844	<0.001*		

https://doi.org/10.1021/acsomega.2c05631
ACS Omega 2022, 7, 41627−41640

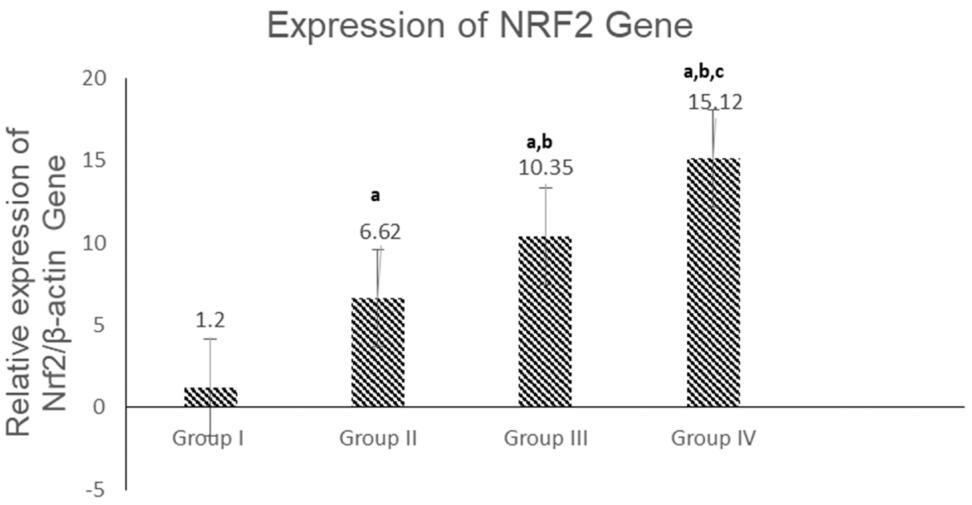

Figure 10. Quantitative measurement of NRF2 gene expression by quantitative real-time reverse transcription PCR (RT-PCR). Fold change of gene expression. (a) significance vs group I, (b) significance vs group II, and (c) significance vs group III.

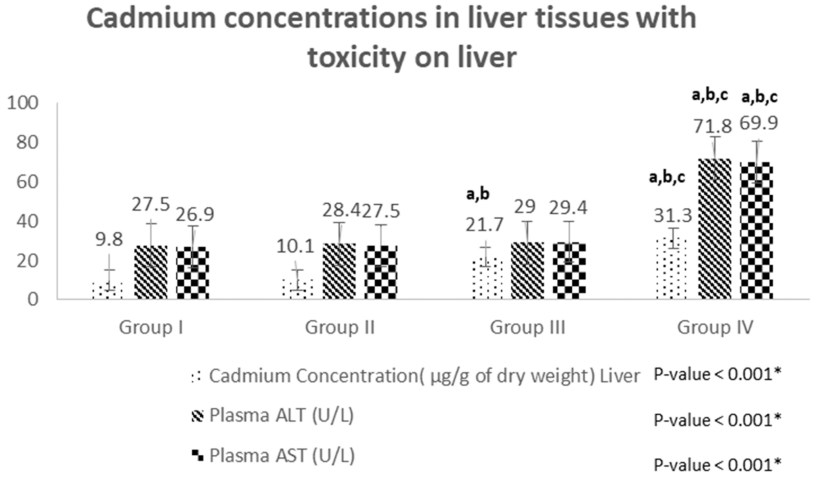

Figure 11. Cadmium concentrations in liver tissues with toxicity on the liver. Values are expressed as mean ± SD. Number of rats in each group (n = 15). P was considered significant at <0.05. (a) Significance vs group I, (b) significance vs group II, and (c) significance vs group III using one-way ANOVA followed by Tukey's post hoc test for multiple comparison.

Table 5. Correlation between Cadmium Concentrations in the Liver and Liver Enzymes among the Different Studied Groups

	plasma ALT (U/L)		plasma AST (U/L)	
	r.	*P*	*r.*	*P*
cadmium concentrations in the liver (μg/g of dry weight) liver	0.92	<0.001*	0.93	<0.001*

on the biodistribution characteristic of the nanoparticle rather than the free drug. The desire for techniques with minimal side effects and more specificity led to the development of nanotechnology-based therapeutics.[41]

Nanoparticles containing cadmium have opened up new possibilities for cancer prevention and treatment for scientists and researchers. Cadmium nanocomplex-based therapy has developed as a novel branch of nano-based therapeutics in this regard.[19]

3.1. Effect of Cd Nanocomplex Therapy on Tumor Growth and Survival Status (after 36 Days). In contrast to the 0% death rate in the control group (group I), five rats died in the EAC group (group II), with a death rate of 33.3%, compared to the 13.3% death rate (two rats) in the EAC treated with low-dose Cd nanocomplex group (group III) and the 20% death rate (three rats) in the EAC treated with high-dose Cd nanocomplex group (group IV). Dead animals were excluded from our study, and 15 mice were used in each group for accurate statistical analysis (Figure 6).

***Statistics were done on 15 mice in each group to unify the numbers in each group.** As shown in Figure 7, the EAC cell viability and the ascetic fluid volume were significantly reduced in the EAC treated with low-dose Cd nanocomplex group (group III) as compared with the EAC group (group II). In addition, there were significant decreases in EAC cell viability and ascetic fluid volume in the EAC treated with high-dose Cd nanocomplex group (group IV) as compared with groups II and III.

Moreover, the cadmium concentration expressed in μg/g of dry weight was significantly higher in the EAC treated with low-dose Cd nanocomplex group (group III) as compared with the control group (group I) and the EAC group (group II). The cadmium concentration was also significantly higher in the

https://doi.org/10.1021/acsomega.2c05631
ACS Omega 2022, 7, 41627−41640

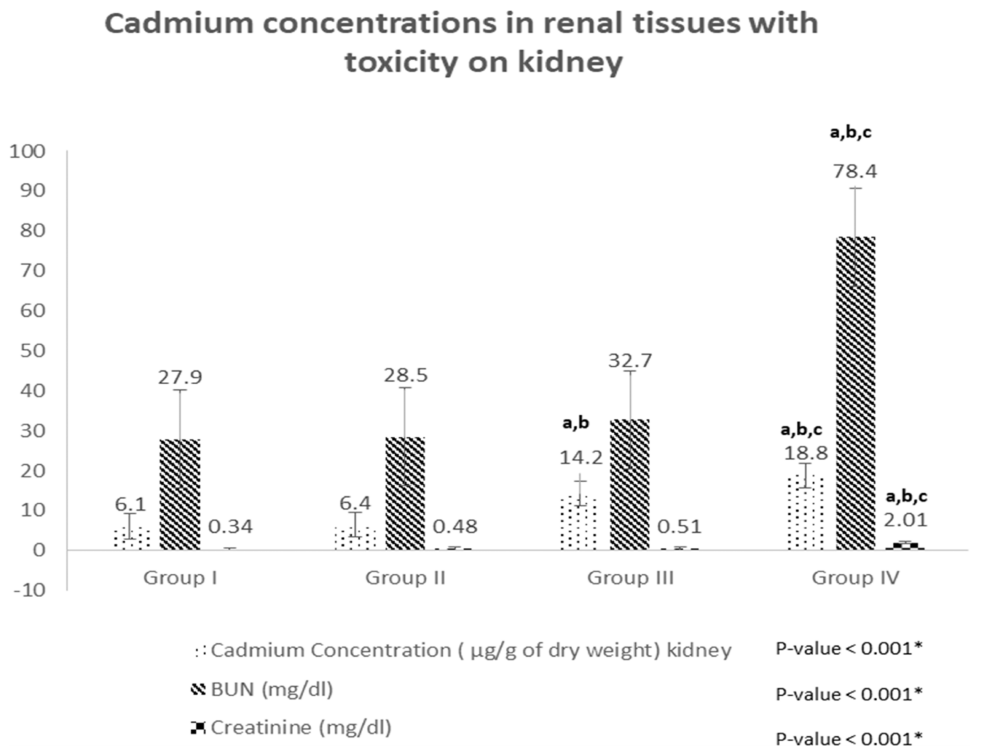

Figure 12. Cadmium concentrations in renal tissues with toxicity on kidney. Values are expressed as mean ± SD. Number of rats in each group (n = 15). P was considered significant at <0.05. (a) Significance vs group I, (b) significance vs group II, and (c) significance vs group III using one-way ANOVA followed by Tukey's post hoc test for multiple comparison.

Table 6. Correlation between Cadmium Concentrations in the Kidney and Renal Function Tests among the Different Studied Groups

	BUN		creatinine	
	r.	*P*	r.	*P*
Cadmium concentrations in the kidney (µg/g of dry weight) kidney	0.688	<0.001*	0.707	<0.001*

EAC treated with high-dose Cd nanocomplex group (group IV) as compared with the other groups (groups I, II, and III). Table 3 shows a negative correlation between cadmium concentrations in EAC cells and the EAC viability & ascites fluid volume among the different studied groups.

This was supported by the findings of Heidari A and Brown C (2015), who concluded that Cd nanocomplexes had anticancer capabilities due to their unique optical, chemical, photoelectrochemical, and electrical properties. Most heavy metals, such as cadmium, have been found to kill cancer cells at low concentrations. The major method of action of the Cd nanocomplex on cancer cells is DNA and protein damage, as well as cell-wall breakdown.[19]

3.2. Effect of Cd Nanocomplex Therapy on Inflammatory, Pyroptosis, Epigenetic Instability, Oxidative Stress, and Antioxidant Biomarkers. There were significant increments in EAC lysate levels of IL-6 (as inflammatory biomarkers), NLRP3 (as a pyroptosis biomarker), 8-OHdG (as an epigenetic instability biomarker), peroxynitrite (as an oxidative stress biomarker), and glutathione peroxidase (as an antioxidant enzyme) in the EAC treated with high-dose Cd nanocomplex group (group IV) as compared with all other studied groups (groups I, II, and III). These biomarkers were significantly elevated in the EAC treated with low-dose Cd nanocomplex group (group III) as compared with groups I and II. Furthermore, these biomarkers were significantly higher in the EAC group (group II) when compared with the control group (group I) (Figures 8 and 9).

Table 4 shows a positive correlation between the different studied biomarkers among the different studied groups.

Noteworthy, Liu et al. (2015) discovered that the activities of antioxidant enzymes such as glutathione peroxidase (GPX), catalase (CAT), and glutathione S-transferase (GST) increased significantly after the treatment with the Cd nanocomplex. In accordance, the transcription status of *superoxide dismutase 1* (*Sod1*), *superoxide dismutase 2* (*Sod2*), catalase (CAT), glutathione peroxidase (GPX), and *heme oxygenase-1* (*Ho1*) were also increased by the high-dose Cd nanocomplex or a long period (21 days) of exposure.[42]

The rate of reactive oxygen species (ROS) formation exceeds the antioxidant enzymes' ability to quench them at high doses of the Cd nanocomplex. As a result, excessive levels of ROS disrupt the cellular machinery, resulting in the oxidation of polyunsaturated fatty acids in lipids (lipid peroxidation), the oxidation of NO with formation of peroxynitrite, and damage of DNA.[43]

The Cd nanocomplex can enhance ROS and RNS formation. The marked rise in tissue MDA along with NO concentration was an indication of the oxidative and nitrosative stress created by Cd-containing nanoparticles. They have the ability to displace iron, resulting in an abundance of free redox-active ions. The Fenton reaction directly boosts the formation of hydroxyl radicals by these free redox metals. They also increase the activity of nicotinamide adenine dinucleotide phosphate (NADPH) oxidase, resulting in the generation of the superoxide anion and the overexpression of inducible nitric oxide synthase, which produces excess NO and active nitrogen

https://doi.org/10.1021/acsomega.2c05631
ACS Omega 2022, 7, 41627−41640

for enhanced lipid peroxidation and peroxynitrite. Nanoparticles containing cadmium significantly increased Bax and Cas-3 while decreasing Bcl2. As a result of the development of the reactive oxygen species (ROS), they have apoptotic features.[44]

Interestingly, Amenah Mohmmad Monadi Al-Enazi et al. (2020) illustrated that the metal-mediated generation of ROS can create severe oxidative damage in nucleic acids, such as strand breaks and base oxidation 8-OHdG. The exposure to Cd-containing nanoparticles showed a marked increment in the levels of 8-OHdG, which corresponds to the Cd-induced oxidative DNA damage, failure of DNA repair, and epigenetic instability.[45]

In vivo effects of the model Cd nanocomplex demonstrated an ongoing inflammatory process caused by circulating inflammatory factors (e.g., IL-6, TGF-ß1) released, together with a general overexpression of IL-6. Cellular localization and distribution of IL-6 and TGF-ß1 revealed an increased expression of these cytokines as evidence of an enhanced cellular inflammatory response after administration of cadmium-containing nanoparticles.[46]

Previous studies have shown that in rat models, the Cd nanocomplex can also induce NLR family pyrin domain containing 3 (NLRP3) inflammasome-dependent pyroptosis in vascular endothelial cells through the generation of ROS and mitochondria reactive oxygen species (mtROS). Activating NLRP3 further promotes the maturation of caspase-1, leading to the release of IL-18, IL-6, IL-1, and other inflammatory factors, which exacerbate inflammatory response. Accumulation of inflammatory cytokines eventually leads to the occurrence of pyroptosis.[47]

Figure 10 shows that there was a significant increase in the Nrf2 mRNA gene expression in the EAC group (group II) when compared with the control group (group I). Additionally, there was a significant increase in Nrf2 mRNA gene expression in the EAC treated with low-dose Cd nanocomplex group (group III) as compared with groups I and II. There was also a significant increase in Nrf2 mRNA gene expression in the EAC treated with high-dose Cd nanocomplex group (group IV) as compared with the other studied groups (groups I, II, and III).

It is tempting to speculate that the nuclear factor Nrf2 (erythroid 2-related factor 2) is a member of the Cap "n" Collar (CNC) subfamily of basic leucine zipper-type transcription factors that plays an important role in maintaining homeostasis. The NRF2 gene is a tumor suppressor because it protects cells from oxidative and electrophilic assaults, making it anticarcinogenic.[48]

The Nrf2/antioxidant response element (ARE) signaling pathway, one of the major antioxidant pathways, is initiated by Nrf2 activation. Because it is linked to Kelch-like ECH-associated protein 1, Nrf2 is normally inactive in the cytosol (keap1). The Nrf2 transcription factor is activated by oxidative stress when it is released from the Nrf2/keap1 complex. The free Nrf2 then travels to the nucleus, where it binds to the ARE and activates antioxidant enzyme-coding targets.[49]

Plausibly, Nrf2 is a cellular protector, and this principle applies to both normal cells and malignant cells. Nrf2 dissociates from its inhibitor, Keap1, and enters the nucleus when the quantity of reactive oxygen species (ROS) rises. Nrf2 regulates an estimated 250 genes in the nucleus, mostly involved in endogenous antioxidant protection in different species. Some of its most important targets include the genes listed: NAD(P)H dehydrogenase (quinone) 1 (NQO1), heme oxygenase-1 (HMOX1), glutathione S-transferase 1 (GST), peroxiredoxins, glutamate−cysteine ligase (GCL), and glutathione (GSH). There is an inverse correlation between Nrf2 and the tumor-promoter transcription factor (TF), the nuclear factor kappa-light-chain-enhancer of activated B cells (NF-κB).[50]

Several studies have shown that Nrf2 has a protective function in a variety of cancers, neurological diseases, cardiovascular problems, aging, inflammation, and photo-oxidative stress.[51]

These results are in agreement with our results herein that documented a significant increase in NRF2 gene expression in the EAC group when compared with the control group. Additionally, there was a significant increase in NRF2 gene expression in the EAC treated with low-dose Cd nanocomplex group (group III) as compared with the control and EAC groups. There was also a significant increase in NRF2 gene expression in the EAC treated with high-dose Cd nanocomplex group (group IV) as compared with the other studied groups (Figure 6).

On the contrary, some other researchers reported the coactivation of Nrf2 and other oncogenic signaling pathways such as phosphoinositide 3-kinases (PI3K), mitogen-activated protein kinase (MAPK), and Notch1. Furthermore, tumor cell multiplication and proliferation have been found to occur as a result of hyperactivation of Nrf2, which stops cancer cells from experiencing apoptosis and cellular death, making them resistant to chemotherapy or radiotherapy.[52]

3.3. Cd Nanocomplex Therapy Effect on Liver Toxicity. As shown in Figure 11, the cadmium concentration was significantly elevated in the EAC treated with low-dose Cd nanocomplex group (group III) as compared with the control group (group I) and the EAC group (group II). The cadmium concentration was also significantly elevated in the EAC treated with high-dose Cd nanocomplex group (group IV) as compared with the other groups (groups I, II, and III). Significant increments in liver enzyme (ALT and AST) activities were evident in the EAC treated with high-dose Cd nanocomplex group (group IV) as compared with the other groups (groups I, II, and III). Furthermore, Table 5 reveals a positive correlation between cadmium concentrations in the liver and increased liver enzyme activities among the different studied groups.

3.4. Cd Nanocomplex Therapy Effect on Renal Toxicity. The cadmium concentration was also significantly higher in the EAC treated with high-dose Cd nanocomplex group (group IV) as compared with the other groups (groups I, II, and III). Moreover, the cadmium concentration was significantly elevated in the EAC treated with low-dose Cd nanocomplex group (group III) as compared with the control group (group I) and the EAC group (group II). Significant increases in levels of renal function tests (BUN and creatinine) were obvious in the EAC treated with high-dose Cd nanocomplex group (group IV) as compared with the other groups (groups I, II, and III), as presented in Figure 12. Likewise, Table 6 shows that cadmium concentrations in the kidney were positively correlated to elevated BUN and creatinine levels among the different studied groups.

Rana et al. (2021) discovered that while recent nanoparticles have been considered to be important for drug delivery systems, cadmium is known to cause hepatic toxicity through oxidative stress, exhaustion of endogenous antioxidants, apoptosis, mitochondrial injury, and intracellular calcium

https://doi.org/10.1021/acsomega.2c05631
ACS Omega 2022, 7, 41627−41640

signaling disturbance.[53] Additionally, Liu et al. (2015) found that in the liver, there were changes in the key biomarkers associated with oxidative stress and inflammatory reactions when given a relatively high dose of cadmium or when given long-term treatment for 21 days, revealing that cadmium exposure could cause immunotoxicity and oxidative stress in the livers of mice. These findings corroborated our findings here: significant increments in liver enzyme (ALT and AST) activities were evident herein in the EAC treated with high-dose cadmium (Cd) nanoparticle group (group IV) as compared with the other groups (Figure 11). Furthermore, Table 5 reveals a positive correlation between cadmium concentrations in the liver and increased liver enzyme activities among the different studied groups.[54]

Likewise, EAC treated with high-dosage cadmium (Cd) nanoparticles (group IV) showed significant increases in renal function tests (BUN and creatinine levels) when compared to other groups (Figure 12). Table 6 further reveals that cadmium concentrations in the kidney were positively correlated with higher BUN and creatinine levels in the various study groups. These findings matched those of Rana et al. (2018), who discovered that cadmium-containing nanoparticles have a higher potential for generating ROS, inducing oxidative stress, and impairing the renal structure and function because they can interact with organelles like mitochondria and generate ROS or interact with redox-active proteins like NADPH oxidase. They have the ability to react with cell surface receptors and activate intracellular signaling pathways, resulting in the induction of oxidative stress.[55]

4. Conclusions. Cadmium nanocomposites have anticancer effects on Ehrlich ascites tumors induced in mice via their effects on the immune system and redox status of the body. They enhance oxidative stress and inflammatory and epigenetic instability biomarkers, stimulating apoptosis together with the activation of pyroptosis. Hence, high doses of cadmium nanocomposites can cause liver and renal toxicity.

AUTHOR INFORMATION

Corresponding Author

Heba Bassiony Ghanem − *Clinical laboratory sciences Department, College of Applied Medical Sciences, Jouf University, Sakaka, Aljouf 2014, Saudi Arabia; Medical Biochemistry Department, Faculty of Medicine, Tanta University, Tanta 31527, Egypt*; orcid.org/0000-0002-7987-5111; Email: hbghanem@ju.edu.sa, heba.ghanem@med.tanta.edu.eg

Authors

Rehab Galal El-Sharkawy − *Chemistry Department, College of Science, Jouf University, Sakaka, Aljouf 2014, Saudi Arabia; Chemistry Department, Faculty of Science, Tanta University, Tanta 31527, Egypt*

Rania Hosny Taha − *Chemistry Department, College of Science, Jouf University, Sakaka, Aljouf 2014, Saudi Arabia; Department of Chemistry, Faculty of Science (Girls), Al-Azhar University, 11754 Nasr City, Egypt*

Complete contact information is available at: https://pubs.acs.org/10.1021/acsomega.2c05631

Funding

The financial support of this study is provided by Jouf University through research project no. (DSR2020-04-449).

Notes

The authors declare no competing financial interest.

ACKNOWLEDGMENTS

The authors extend their appreciation to the Deanship of Scientific Research at Jouf University for funding this work through research grant no (DSR2020-04-449).

REFERENCES

(1) Dermeche, S.; Nadour, M.; Larroche, C.; Moulti-Mati, F.; Michaud, P. Olive mill wastes: Biochemical characterizations and valorization strategies. *Process Biochem.* **2013**, *48*, 1532−1552.

(2) Kartesz, J.*The Biota of North America Program (BONAP)*; North American Plant Atlas: Chapel Hill, NC, 2011.

(3) Alshammari, B. A.; Alotaibi, M. D.; Alothman, O. Y.; Sanjay, M. R.; Kian, L. K.; Almutairi, Z.; Jawaid, M. A new study on characterization and properties of natural fibers obtained from olive tree (Olea europaea L.) residues. *J. Polym. Environ.* **2019**, *27*, 2334−2340.

(4) El-Kholy, M.; Avanzato, D.; Caballero, J.; Chartzoulakis, K.; Vita Serman, F.; Perry, E.*Following Olive Footprints (Olea europaea L.)-Cultivation and Culture, Folklore and History, Tradition and Uses*; International Society for Horticultural Science (ISHS), 2012.

(5) Al Arabi, K.; Elamri, N.; Elgariani, N.; Diab, K.; Elriani, A.; Eldoungli, E.The antagonistic effects of culture filtrate of local isolates of Trichoderma spp. against some olive trees fungal pathogens. In *Proceeding of the Symposium International sur la Protection intégrée de l'olivier*, 2008.

(6) Butt, T. M.; Jackson, C.; Magan, N.*Fungi as Biocontrol Agents: Progress Problems and Potential*; CABI, 2001.

(7) Saremi, H.; Eskandar, Z.Fungi and biological control, pests, pathogens, herbsZanjan University Publication, 2003; Vol. *142*.

(8) D'Amore, A.; Grassia, L.; Acierno, D. In *6th International Conference on Times of Polymers (ToP) and Composites*2012; Vol. 1459.

(9) Asgari, M.; Sundararaj, U. Silane functionalization of sodium montmorillonite nanoclay: The effect of dispersing media on intercalation and chemical grafting. *Appl. Clay. Sci.* **2018**, *153*, 228−238.

(10) Zhang, J.; Gupta, R. K.; Wilkie, C. A. Controlled silylation of montmorillonite and its polyethylene nanocomposites. *Polymer* **2006**, *47*, 4537−4543.

(11) Zanetti, M.; Lomakin, S.; Camino, G. Polymer layered silicate nanocomposites. *Macromol. Mater. Eng.* **2000**, *279*, 1−9.

(12) Huskić, M.; Žigon, M.; Ivanković, M. Comparison of the properties of clay polymer nanocomposites prepared by montmorillonite modified by silane and by quaternary ammonium salts. *Appl. Clay. Sci.* **2013**, *85*, 109−115.

(13) El-Sharkawy, R. G.; Taha, R. H.; Ghanem, H. B. Immobilization of novel inorganic nano-complexes onto MWCNT nanomaterials as a novel adsorbent and anti-inflammatory therapy in an induced model of rheumatoid arthritis. *Nanotechnology* **2020**, *31*, No. 305706.

(14) Sim, S.; Wong, N. Nanotechnology and its use in imaging and drug delivery. *Biomed. Rep.* **2021**, *14*, No. 42.

(15) Raj, S.; Khurana, S.; Choudhari, R.; Kesari, K. K.; Kamal, M. A.; Garg, N.; Ruokolainen, J.; Das, B. C.; Kumar, D.Specific targeting cancer cells with nanoparticles and drug delivery in cancer therapy. In *Seminars in Cancer Biology*; Elsevier, 2021; Vol. *69*, pp 166−177.

(16) Al-Rasheed, N. M.; El-Masry, T. A.; Tousson, E.; Hassan, H. M.; Al-Ghadeer, A. J. B. J. o. P. S. Hepatic protective effect of grape seed proanthocyanidin extract against Gleevec-induced apoptosis, liver Injury and Ki67 alterations in rats. *Braz. J. Pharm. Sci.* **2018**, *54*, No. e17391.

(17) Lefojane, R. P.; Sone, B.; Matinise, N.; Saleh, K.; Direko, P.; Mfengwana, P.; Mashele, S.; Maaza, M.; Sekhoacha, M. P. CdO/CdCO3 nanocomposite physical properties and cytotoxicity against selected breast cancer cell lines. *Sci. Rep.* **2021**, *11*, No. 30.

(18) Ghanem, H. B. Impact of zinc oxide nanoparticles and thymoquinone in Ehrlich ascites carcinoma induced in mice. *J. Biochem. Mol. Toxicol.* **2021**, *35*, No. e22736.
(19) Heidari, A.; Brown, C. Study of composition and morphology of cadmium oxide (CdO) nanoparticles for eliminating cancer cells. *J. Nanomed. Res.* **2015**, *2*, No. 00042.
(20) Nguyen, K. C.; Seligy, V. L.; Massarsky, A.; Moon, T. W.; Rippstein, P.; Tan, J.; Tayabali, A. F.Comparison of toxicity of uncoated and coated silver nanoparticles. In *Journal of Physics: Conference Series*; IOP Publishing: Vol. 2013; Vol. *429*, p 012025 DOI: 10.1088/1742-6596/429/1/012025.
(21) Zhang, Y.; Liu, Q.; Yin, H.; Li, S. Cadmium exposure induces pyroptosis of lymphocytes in carp pronephros and spleens by activating NLRP3. *Ecotoxicol. Environ. Saf.* **2020**, *202*, No. 110903.
(22) Salam, H. A.; Rajiv, P.; Kamaraj, M.; Jagadeeswaran, P.; Gunalan, S.; Sivaraj, R. Plants: green route for nanoparticle synthesis. *Int. Res. J. Biol. Sci.* **2012**, *1*, 85−90.
(23) Louis, K. S.; Siegel, A. C.Cell viability analysis using trypan blue: manual and automated methods. In *Mammalian Cell Viability*; Springer, 2011; pp 7−12.
(24) Yılmaz, S.; Ülger, H.; Ertekin, T.; Yay, A. H.; Nisari, M.; Alpa, Ş.; Acer, N. Investigating the anti-tumoral effect of curcumin on the mice in which Ehrlich ascites and solid tumor is created. *Iran. J. Basic Med. Sci.* **2019**, *22*, 418−425.
(25) Jin, Y.; Zhang, S.; Tao, R.; Huang, J.; He, X.; Qu, L.; Fu, Z. Oral exposure of mice to cadmium (II), chromium (VI) and their mixture induce oxidative-and endoplasmic reticulum-stress mediated apoptosis in the livers. *Environ. Toxicol.* **2016**, *31*, 693−705.
(26) Takahashi, S.; Takahashi, I.; Sato, H.; Kubota, Y.; Yoshida, S.; Muramatsu, Y. Determination of major and trace elements in the liver of Wistar rats by inductively coupled plasma-atomic emission spectrometry and mass spectrometry. *Lab. Anim.* **2000**, *34*, 97−105.
(27) Bradford, M. M. A rapid and sensitive method for the quantitation of microgram quantities of protein utilizing the principle of protein-dye binding. *Anal. Biochem.* **1976**, *72*, 248−254.
(28) Beckman, J. S.; Ischiropoulos, H.; Zhu, L.; van der Woerd, M.; Smith, C.; Chen, J.; Harrison, J.; Martin, J. C.; Tsai, M. Kinetics of superoxide dismutase-and iron-catalyzed nitration of phenolics by peroxynitrite. *Arch. Biochem. Biophys.* **1992**, *298*, 438−445.
(29) VanUFFELEN, E. B.; Van der ZEE, J.; de KOSTER, M. B.; VanSTEVENINCK, J.; Jan ELFERINK, G. R. Intracellular but not extracellular conversion of nitroxyl anion into nitric oxide leads to stimulation of human neutrophil migration. *Biochem. J.* **1998**, *330*, 719−722.
(30) Paglia, D. E.; Valentine, W. N. Studies on the quantitative and qualitative characterization of erythrocyte glutathione peroxidase. *J. Lab. Clin. Med.* **1967**, *70*, 158−169.
(31) El-Magd, M. A.; Abdo, W. S.; El-Maddaway, M.; Nasr, N. M.; Gaber, R. A.; El-Shetry, E. S.; Saleh, A. A.; Alzahrani, F. A. A.; Abdelhady, D. H. High doses of S-methylcysteine cause hypoxia-induced cardiomyocyte apoptosis accompanied by engulfment of mitochondaria by nucleus. *Biomed. Pharmacother.* **2017**, *94*, 589−597.
(32) Livak, K. J.; Schmittgen, T. D. Analysis of relative gene expression data using real-time quantitative PCR and the 2(-Delta Delta C(T)) Method. *Methods* **2001**, *25*, 402−408.
(33) Taha, R. H.; El-Shafiey, Z. A.; Salman, A. A.; Mansour, M. M. A study of a newly synthesized ligand and its metal complexes in bulk and nano size and metal uptake efficiency. *Appl. Organomet. Chem.* **2020**, *34*, No. e5792.
(34) Moustafa, S. M. N.; Taha, R. H.; Abdelzaher, H. M. A.; Elgebaly, H. A. Novel biosynthesis of Ag-nanocomplex for controlling Verticillium wilt disease of olive tree. *Arch. Phytopathol. Plant Prot.* **2022**, *55*, 198−216.
(35) Feiz, S.; Navarchian, A. H. Poly(vinyl alcohol) hydrogel/chitosan-modified clay nanocomposites for wound dressing application and controlled drug release. *Macromol. Res.* **2019**, *27*, 290−300.
(36) Abramov, D.; Arakelian, S.; Kochuev, D.; Makov, S.; Prokoshev, V.; Khorkov, K. Interaction of femtosecond laser radiation with carbon materials: exfoliation of graphene structures and synthesis of low-dimensional carbon structures. *Nanosyst.: Phys., Chem., Math.* **2016**, *7*, 220−225.
(37) Cankaya, N.; Sahin, R. Chitosan/clay bionanocomposites: Structural, antibacterial, thermal and swelling properties. *Cellulose Chem. Technol.* **2019**, *53*, 537−549.
(38) Aldubayan, M. A.; Elgharabawy, R. M.; Ahmed, A. S.; Tousson, E. Antineoplastic activity and curative role of avenanthramides against the growth of ehrlich solid tumors in mice. *Oxid. Med. Cell. Longevity* **2019**, *2019*, 1−12.
(39) Kabel, A. M.; Abdel-Rahman, M. N.; El-Sisi, A. E.-D. E.; Haleem, M. S.; Ezzat, N. M.; El Rashidy, M. A. Effect of atorvastatin and methotrexate on solid Ehrlich tumor. *Eur. J. Pharmacol.* **2013**, *713*, 47−53.
(40) Abd Eldaim, M. A.; Tousson, E.; El Sayed, I. E. T.; Abd Elmaksoud, A. Z.; Ahmed, A. A. S. Ameliorative effects of 9-diaminoacridine derivative against Ehrlich ascites carcinoma−induced hepatorenal injury in mice. *Environ. Sci. Pollut. Res.* **2021**, *28*, 21835−21850.
(41) Sharma, G.; Singh, M.; Sharma, K.; Sharma, P.; Mehra, S.*Role of Nanotechnology in Cancer Treatment. Importance & Applications of Nanotechnology*; MedDocs Publishers, 2021.
(42) Liu, L.; Tao, R.; Huang, J.; He, X.; Qu, L.; Jin, Y.; Zhang, S.; Fu, Z. Hepatic oxidative stress and inflammatory responses with cadmium exposure in male mice. *Environ. Toxicol. Pharmacol.* **2015**, *39*, 229−236.
(43) Gao, M.; Yang, Y.; Lv, M.; Song, W.; Song, Z. Oxidative stress and DNA damage in zebrafish liver due to hydroxyapatite nanoparticles-loaded cadmium. *Chemosphere* **2018**, *202*, 498−505.
(44) Li, X.; Jiang, X.; Sun, J.; Zhu, C.; Li, X.; Tian, L.; Liu, L.; Bai, W. Cytoprotective effects of dietary flavonoids against cadmium-induced toxicity. *Ann. N. Y. Acad. Sci.* **2017**, *1398*, 5−19.
(45) Mohmmad Monadi Al-Enazi, A.; Virk, P.; Hindi, A.; Awad, M. A.; Elobeid, M.; Qindeel, R. Protective effect of probiotic bacteria and its nanoformulation against cadmium-induced oxidative stress in male Wistar rat. *J. King Saud Univ. − Sci.* **2020**, *32*, 3045−3051.
(46) Coccini, T.; Barni, S.; Mustarelli, P.; Locatelli, C.; Roda, E. One-month persistence of inflammation and alteration of fibrotic marker and cytoskeletal proteins in rat kidney after Cd-doped silica nanoparticle instillation. *Toxicol. Lett.* **2015**, *232*, 449−457.
(47) Zhang, Y.; Liu, Q.; Yin, H.; Li, S. Cadmium exposure induces pyroptosis of lymphocytes in carp pronephros and spleens by activating NLRP3. *Ecotoxicol. Environ. Saf.* **2020**, *202*, No. 110903.
(48) Oshi, M.; Angarita, F. A.; Tokumaru, Y.; Yan, L.; Matsuyama, R.; Endo, I.; Takabe, K. High Expression of NRF2 Is Associated with Increased Tumor-Infiltrating Lymphocytes and Cancer Immunity in ER-Positive/HER2-Negative Breast Cancer. *Cancers* **2020**, *12*, 3856.
(49) ALBASHER, G.; ALBRAHIM, T.; ALJARBA, N.; ALHARBI, R. I.; ALSULTAN, N.; ALSAIARI, J.; RIZWANA, H. Involvement of redox status and the nuclearrelated factor 2 in protecting against cadmiumin induced renal injury with Sana Makki (Cassia senna L.) pre-treatment in male rats. *An. Acad. Bras. Ciênc.* **2020**, *92*, No. 20191237.
(50) Zimta, A.-A.; Cenariu, D.; Irimie, A.; Magdo, L.; Nabavi, S. M.; Atanasov, A. G.; Berindan-Neagoe, I. The Role of Nrf2 Activity in Cancer Development and Progression. *Cancers* **2019**, *11*, 1755.
(51) Jaramillo, M. C.; Zhang, D. D. The emerging role of the Nrf2-Keap1 signaling pathway in cancer. *Genes Dev.* **2013**, *27*, 2179−2191.
(52) Bai, X.; Chen, Y.; Hou, X.; Huang, M.; Jin, J. Emerging role of NRF2 in chemoresistance by regulating drug-metabolizing enzymes and efflux transporters. *Drug Metab. Rev.* **2016**, *48*, 541−567.
(53) Rana, K.; Verma, Y.; Rana, S. V. S. Possible Mechanisms of Liver Injury Induced by Cadmium Sulfide Nanoparticles in Rat. *Biol. Trace Elem. Res.* **2021**, *199*, 216−226.
(54) Liu, L.; Tao, R.; Huang, J.; He, X.; Qu, L.; Jin, Y.; Zhang, S.; Fu, Z. Hepatic oxidative stress and inflammatory responses with cadmium exposure in male mice. *Environ. Toxicol. Pharmacol.* **2015**, *39*, 229−236.

https://doi.org/10.1021/acsomega.2c05631
ACS Omega 2022, 7, 41627−41640

(55) Rana, K.; Verma, Y.; Rana, V.; Rana, S. V. S. Renal toxicity of nanoparticles of cadmium sulphide in rat. *Chemosphere* **2018**, *193*, 142−150.

https://doi.org/10.1021/acsomega.2c05631
ACS Omega 2022, 7, 41627−41640